# Nonlinear Optical Properties of Silver Nanoparticles Produced by Laser Ablation

**Bita Azemoodeh Afshar, Akbar Jafari, Rahim Naderali*, and Mir Maqsood Golzan**

**Physics Department, Faculty of Sciences, Urmia University, Urmia, Iran**
***Corresponding author email:** r.naderali@urmia.ac.ir

**Regular paper:** Received: Dec. 29, 2022, Revised: May. 08, 2023, Accepted: May. 13, 2023,
Available Online: May. 15, 2023, DOI: 10.52547/ijop.16.2.187

**Abstract—In this study, we investigated the production of silver nanoparticles by pulsed Nd: YAG laser ablation with λ=532nm in distilled water. The sodium citrate used to control the size of nanoparticles (Nps). The sample containing Ag NPs was characterized by linear absorption spectroscopy (UV-Visible spectroscopy) and transmission electron microscopy (TEM observation). The behavior of nonlinear optical properties of silver nanoparticles was studied using the Z-Scan method at two optimum numbers of the laser pulses and four optimum laser energy densities. In the Z-Scan method, the nonlinear thermal properties of Ag NPs were investigated under exposure to nanosecond laser pulse at λ=532nm. They were gained by fitting theoretical and experimental data. The values of the nonlinear refractive index ($n_2$) and the nonlinear absorption coefficient ($\beta$) were compared concerning to two optimum numbers and four optimum energy densities. The results of the nonlinear refractive index showed a negative value for each sample, this means that samples act as a divergent lens, and the thermal self-defocusing effect can be the main factor of nonlinear behavior. Following the comparison of two quantities, $n_2$ and $\beta$, we found that the nonlinear refractive index increased when the number of laser pulses light increased. In addition, the nonlinear absorption coefficient decreased when the number of laser pulses light increased. As a result, the application of these Ag NPs for optical switching devices was investigated, which demonstrated that the large Ag NPs are applicable tools for optical switching devices.**

**KEYWORDS:** Laser ablation, Nonlinear Optical properties, Size of Silver nanoparticles, Z-scan method.

## I. INTRODUCTION

Metal nanoparticles (Nps) have attractive physical and chemical properties depending on their size. Laser ablation was first performed in the water by Patel and Phase in 1987 [1]. The chemical methods used in the formation of metal nanoparticles. Laser ablation of solids in liquid environments is an alternative method due to its relatively simple experimental setup. The approach enables the possibility of metal nanoparticles' growth in a controllable environment, which is a crucial step for a successfully functionalizing of the metal nanoparticle surface. This method produces metal nanoparticles with high purity in a vacuum, gas, or liquid environment (Atile *et al.* 1987, Ivanchenko *et al.* 2004, Popovici *et al.* 2006, Gómez *et al.* 2007, Brito-Silva *et al.* 2007, Jimenez *et al.* 2010). Furthermore, laser ablation is the fastest and safest method to produce colloidal nanoparticles in a liquid environment with different optical and structural characterizations. Kamalov *et al.* 2002 reported Ag NPs which were produced under picosecond and nanosecond radiations (λ=532nm) without stabilizers. Nonlinear susceptibility changes were studied [4]. Martin *et al.* 2007 produced Ag NPs by second harmonic Q-switched Nd:YAG laser. The effect of nanoparticle size on linear optics was studied [3]. Gonzalez-Castollo *et al.* 2017 reported the synthesis of Ag NPs by laser ablation without stabilizers in two steps. In the first step, silicon NPs had been produced by laser ablation and in the second step the silver salt and HAuCl4 were added. The Ag NPs were produced by redox reaction between silicon NPs and silver and gold ions. The obtained

[ Downloaded from ijop.ir on 2026-11-24 ]

average diameter of NPs was 14nm [5]. The researches that have been reported so far for the production of NPs by laser ablation, has been using one laser energy density and one number of the laser pulses at different times without adding a stabilizer. So that the average size of NPs has large values. In this work, the stabilizer acted like a soft template and keeps the NPs apart and prevent the NPs from merging. As a result, the size of NPs becomes smaller. By changing the laser energy density and the number of laser pulses, we obtained the best mode for producing NPs with much smaller dimensions. For the production of NPs with dimensions of 1.15 nm, 5.04 nm, 6.34 nm and 7.34 nm, the best laser energy densities were obtained 0.015 J/cm$^2$, 0.11 J/cm$^2$, 0.09 J/cm$^2$ and 0.02 J/cm$^2$, respectively. The best numbers of laser pulses were 900 and 1500. In addition, the Changes in nonlinear refractive indices and nonlinear absorption coefficients have been investigated for small NPs. Since the average size of NPs is showed small values, the nonlinear parameters show larger values (it is $10^7$ orders of magnitude larger than what has been reported for the nonlinear refractive index in previous researches) than those previously reported in articles [3, 5, 11].

Metal nanoparticles have unique optical and electrical properties concerning their sizes and shapes in fabricating optical chips and memories. Metal NPs have been extensively studied for their application as an optical limiter under exposure to laser pulse at 532nm wavelength due to the enhancement in nonlinear optical properties [2-3]. These studies were performed using the Z-scan method on the experimental sample. The Z-scan method can be used to measure the nonlinear refractive index and nonlinear absorption coefficient. This technique is a simple and high sensitive method for measuring the nonlinear refractive index and nonlinear absorption coefficient. Various studies have displayed the result of Z-scan measurements by the thermal concave (convex) lens in the medium around the metal NPs due to the tangible heat transfer from the metal NPs to the medium or by the difference between the refractive index of metal NPs and the medium [4].

Silver nanoparticles have different applications depending on their physical properties, such size and shape [6]. These nanoparticles used as antibacterial substances and gene carriers in the biomedical domain. Interestingly, it demonstrates that some antibacterial, optical, and catalytic properties of Ag NPs are enhanced for particle sizes smaller than 15nm. Thus, despite the high surface area and tendency to agglomerate and aggregate, obtaining highly stable Ag NPs smaller than 15nm in a controlled environment has attracted significant interest from the scientific community [7]. In recent years, Nicolae-Maranciuc *et al.* [8] produced Ag NPs by laser ablation without stabilizers. The average diameter of NPs with the shape of spherical is 100-200 nm. Chen *et al.* [9] produced Ag NPs by laser ablation. The average diameter of NPs with the shape of catenary structure is 1.66 nm. In this work, we produced the smaller Ag NPs with a stabilizer for controlling the size of Ag NPs. The obtained average diameters of NPs with the shape of spherical are 1.15-7.34 nm produced by Nd: YAG laser at laser ablation wavelength of 532nm.

Based on the literature [5], agents affect the type and size of nanoparticles and can protect the NP core from aggregation. In addition, the agents can improve the stability related to the lifetime of nanoparticles used for different applications. De Goes *et al.* [10] used sodium citrate as a stabilizer, and capping Ag NPs in water solution to detect the amount of glyphosate (Glyphosate is used for weed control in gardens, that the increase in glyphosate endangers human health) by laser ablation method.

The other important application of these nanoparticles is in biosensors and electronic nanodevices [6]. Plasmon properties of these nanoparticles make them usable in Plasmon sensors [6, 11]. Optical absorption spectra of metal nanoparticles are dominated by surface-Plasmon resonance (SPR). The peak of these spectra shifts to longer wavelengths with an increase in particle size. Their Plasmon resonance is located in the visible region. Silver nanoparticles have an advantage over other

[ Downloaded from ijop.ir on 2026-11-24 ]

nanoparticles because of their surface Plasmon energy located far from the interband transition energy. Silver NPs have a Plasmon resonance of around 400 nm depending on their size and shape [6].

In this study, we aimed to produce silver nanoparticles with an average size smaller than 15nm by laser ablation in distilled water. We also used 1mg of the sodium citrate for stabilization purposes. Particle size was controlled by increasing or decreasing the energy density and the number of the laser pulses. The samples were characterized using linear absorption spectroscopy (UV-Visible spectroscopy) and transmission electron microscopy (TEM observation). Nonlinear optical properties were measured under exposure to nanosecond laser pulse at 532nm wavelength. Nonlinear properties of Ag NPs, including nonlinear refractive and nonlinear absorptive indices, were studied. The theoretical analysis based on the Sheik-Bahaee's model is in agreement with the experimental results of the Z-scan method. Finally, two figures of merit ($|w| \gg 1$ and $|T| \ll 1$ ) were investigated to evaluate the applications of the Ag NPs in all-optical switching devices [17].

## II. EXPERIMENT

### A. *Laser ablation for producing Ag nanoparticles*

The experimental setup for producing Ag NPs by laser ablation is shown in Fig. 1. The silver plate (99.9%) is located at the bottom of a Teflon vessel, filled with distilled water and 1mg of the sodium citrate as a stabilizer. The surface of the silver plate is $1cm^2$, the volume of distilled water is 2.8cc, and the diameter of the vessel is 1.6cm.

The preparation was performed in an open-air condition. The Q-switched Nd: YAG laser system with a pulse duration of 4ns and two optimum numbers of the laser pulses 1500 and 900 used to prepare Ag NPs. The optical power was measured employing an optical power meter. The Nd: YAG laser's second harmonic (532nm) output used as an irradiation source.

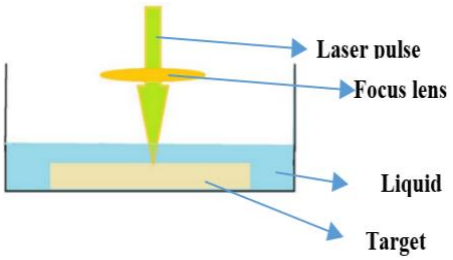


Fig. 1. The experimental arrangement for producing Ag NPs by laser ablation.

### B. *Ag nanoparticles characterization*

After each ablation, 2.8cc of the nanoparticle solution put into a quartz cell with a width of 1cm for the UV-Visible optical spectral characterization. The absorption spectrum of the Ag NPs recorded with a named-HALO XB-10 spectrophotometer. The linear absorption coefficients were obtained by [15]:

$$\alpha_0 = -\frac{1}{L} LnT \qquad (1)$$

$L$=1cm is the cell thickness, and $T$ is the light transmission.

Morphology (the particle size and size distribution) of the prepared samples was obtained with the TEM (Philips BioTwin, the Netherlands) method. For carrying TEM measurements, a drop of the solution containing Ag NPs was deposited and dried on a carbon-coated copper grid.

### C. *Z-scan setup*

Nonlinear properties of the Ag NPs, such as nonlinear absorption coefficient and nonlinear refractive index, were measured using the Z-scan method. The setup of the Z-scan is shown in Fig. 2.

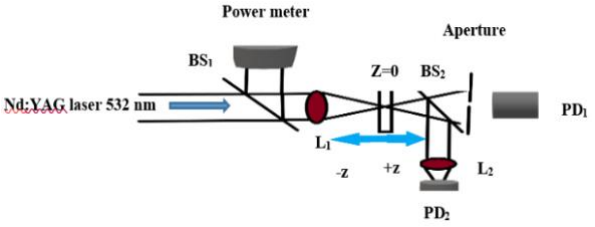


Fig. 2. Arrangement of Z-scan method.

The Z-scan method consists of a continuous-wave diode-pumped laser with $\lambda = 532$nm, laser energy of 64 mJ and output power of 64mW, pinhole, lens (f=10cm), travel linear

[ Downloaded from ijop.ir on 2026-11-24 ]

stage (z-axis), quartz cell with a width of 2mm, and two photodiodes. The TEM00 mode of the laser beam was Focused by a lens with a focal length of $f$=10cm.

The cell has moved along the z-axis, and the nonlinear optical data of refractive index and absorption coefficient have been recorded by two photodiodes, $PD_1$ and $PD_2$. The fraction of diffracted intensity has been measured by $PD_1$ in the close aperture. When a high-intensity of laser beam passed through a nonlinear material, according to the dependence of refractive index on the radiation, $n=n_0+n_2I$, $n_2>0$ ($n_2<0$) resulted in self-focusing (self-defocusing).

For $n_2<0$ when the sample was at front of the focal point of the lens, the transverse section of the laser beam (due to the self-defocusing effect) became enlarged in the aperture in $PD_1$. Which led to formation of a peak in the $z<0$ zones and a valley in the $z>0$ zones. In addition, when the sample was behind the focal point of the lens, the self-defocusing effect caused the transverse section of laser beam to be more minor in the aperture, which led to the formation of a valley in the $z>0$ zones. For $n_2>0$, we have a valley in the transmittance of the aperture when the sample scanned in the $z<0$ zones and a peak in the $z>0$ zones, respectively [12].

The theoretical data obtained using the Sheik-Bahaee's model for nonlinear optical parameters [16]. In addition to the contribution of the data related to the nonlinear refractive index, the data related to the nonlinear absorption coefficient is also involved in $PD_1$. To eliminate the nonlinear absorption coefficient effect, the data of detector $PD_1$ were divided by the data of detector $PD_2$ by point by-point. Then, all the new data were normalized to the transmittance of the close aperture when no sample was present. The normalized peak to valley transmittance for close aperture, $\Delta T(z)$, is given as [12-16]:

$$\Delta T(z) = 1 - \frac{4\Delta\varphi_0 x}{(x^2+1)(x^2+9)} \quad (2)$$

in which $x$ is the normalized distance ($x = z/z_0$) and $z_0$ is the Rayleigh length. The nonlinear phase shift, $\Delta\varphi_0$, which is related to the nonlinear refractive index $n_2$, is [12-16]:

$$n_2 = \frac{\Delta\varphi_0}{kL_{eff}I_0} \quad (3)$$

in which $k = \frac{2\pi}{\lambda}$ is the wave number, $L_{eff} = \frac{1-e^{\alpha_0 L}}{\alpha_0}$ is the effective length of the nonlinear medium, $I_0$ is the on-axis irradiance at the focal of the lens, and L=2mm is the sample thickness at Z-scan.

The photodiode, $PD_2$, measured the intensity dependence on absorption in the open aperture. When the sample was moved along the z-axis and passed through the focal point of the lens, the intensity of the laser increased at the cross - section of the beam and the data were recorded by $PD_2$ that showed a valley (peak) at the position $z$=0 for $\beta > 0$ ($\beta < 0$). This phenomenon was due to the dependence of the absorption coefficient on the laser intensity, $\alpha = \alpha_0 + \beta I$.

As a result, for $\beta > 0$, we have a valley due to nonlinear two-photon absorption, and for $\beta<0$, we have a peak due to nonlinear saturation absorption [9]. All the data were normalized to the transmittance of open aperture when no sample was present. The normalized transmittance for the open aperture is given as [12-16]:

$$T(z) = 1 - \frac{q_0}{2\sqrt{2}(1+x^2)} \quad (4)$$

Moreover, the nonlinear phase shift, $q_0$, which is related to the nonlinear absorption coefficient $\beta$, is [12-16]:

$$q_0 = \beta I_0 L_{eff} \quad (5)$$

### D. *Two figures of merit*

The Ag NPs suitable candidates for optical switching devices due to the presence of delocalized π-electron, and the transforming electron densities between the Ag NPs and ligands. For the application of the Ag NPs in all-optical switching devices, we used the following two figures of merit [17]:

[ Downloaded from ijop.ir on 2026-11-24 ]

$$W = \frac{n_2 I_0}{\alpha_0 \lambda} \quad (6)$$

and

$$T = \frac{\beta \lambda}{n_2} \quad (7)$$

where $\lambda$ is the wavelength at Z-scan. For the suitability of these NPs in all-optical devices, it is necessary to obtain $|W| \gg 1$ and $|T| \ll 1$ [17].

## III. Results and Discussion

### A. *Ag Nanoparticles characterization*

Figures 3 and 4 show the UV-visible spectrum of nanoparticle solution prepared by ablating an Ag target in 2.8cc distilled water and 1mg of the sodium citrate through focusing laser light. The spot size was found to be 1mm. The optimum ablation time was found to be 5 minutes. This was the based on the fact that the distribution of Ag NPs is lower than 5min, and there is no absorption peak less than 5 min. Sodium citrate was used as a capping/stabilization agent or soft template to control the size of Ag NPs [18].

The interaction between sodium citrate and Ag+ was strong (interaction between Ag+ ions and COO- and OH groups in sodium citrate formula and water). The aqueous solution contained Ag+ ions, COO-, and OH groups. The vapor of Ag NPs or silver plasma was produced by laser ablation. During ablation, sodium citrate and water started to decompose by ablating laser and sodium citrate caps Ag0 and Ag+ ions. Different number of the laser pulses per constant energy density (laser energy density describes the optical energy delivered per unit of area) were tested in laser ablation to produce Ag NPs ranging from 300 to 6000. However, Ag NPs were not produced for a constant energy density and different numbers of the laser pulse. In addition, different energy densities per constant number of the laser pulses were tested in laser ablation to produce Ag NPs from 0.007J/cm$^2$ to 0.127J/cm$^2$. However, the optimum number of the laser pulses for producing Ag NPs was 900 and greater. Ag NPs were not produced at numbers less than 900. Figures 3 and 4 show some attempts for producing Ag NPs. In Figs. 3 and 4, nanoparticles produced at the same time under the same conditions.

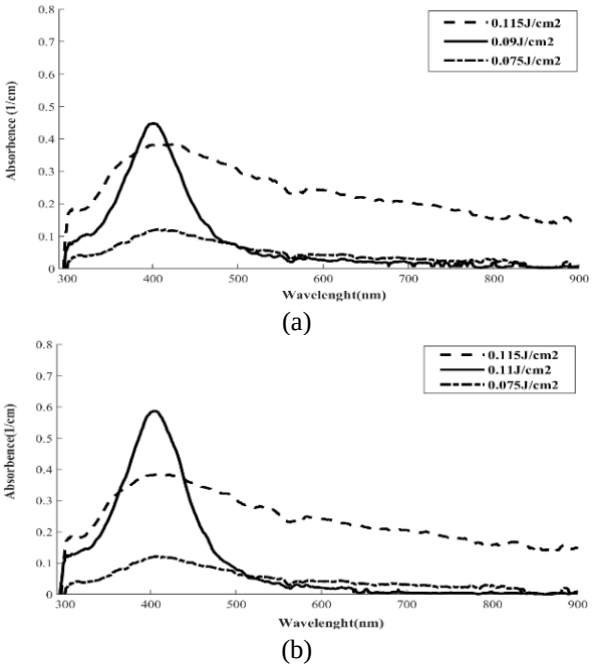


Fig. 3. UV-visible spectrum of Ag NPs at the number of the laser pulses at 900 and (a) three different laser energy densities: 0.115J/cm$^2$ and 0.09J/cm$^2$ and 0.075J/cm$^2$ (b) three different laser energy densities: 0.115J/cm$^2$ and 0.11J/cm$^2$ and 0.075J/cm$^2$.

As shown in Fig. 3(a), the UV-visible peaks for the 900 numbers of the laser pulses at three different laser energy densities: 0.115 J/cm$^2$ and 0.09 J/cm$^2$, and 0.075 J/cm$^2$ appeared at about λ= 411 nm and λ= 404 nm and λ=410 nm, respectively. Since the surface Plasmon resonance occurred at higher wavelengths for large Ag NPs [19-20], the size of Ag NPs at 0.09 J/cm$^2$ is the smallest of the three laser energy densities. On the other hand, the increase of the absorption peak intensity can be related to the increase in concentration of Ag NPs in the solution, which as indicated, the concentration of Ag NPs at 0.09 J/cm$^2$ is higher than the other two laser energy densities. As a result, the optimum laser energy density for producing Ag NPs at the number of the laser pulses at 900 was 0.09 J/cm$^2$.

According to the above (description of Fig. 3(a)), the UV-visible peaks in Fig.3b for the 900 numbers of the laser pulses at three different laser energy densities: 0.115 J/cm$^2$ and 0.11 J/cm$^2$, and 0.075 J/cm$^2$ appeared at about λ=

[ Downloaded from ijop.ir on 2026-11-24 ]

411 nm and λ=401 nm and λ=410 nm, respectively. As a result, the optimum laser energy density for producing Ag NPs at the number of the laser pulses at 900 was 0.11 J/cm$^2$.

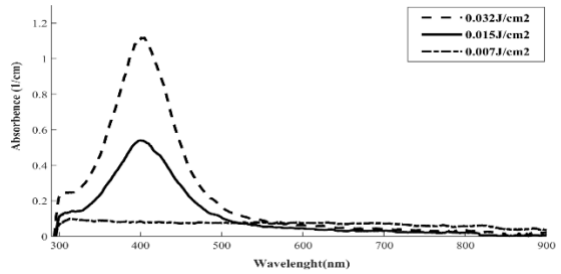


(a)

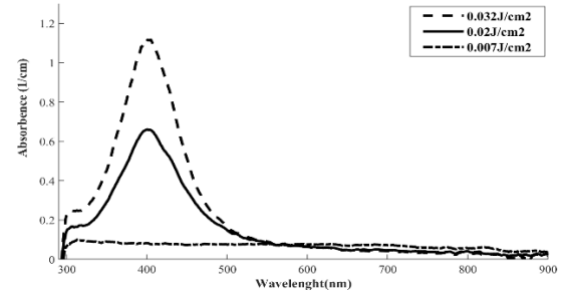


(b)

Fig. 4. UV-visible spectrum of Ag NPs at the number of the laser pulses at 1500 and (a) three different laser energy densities: 0.032J/cm$^2$ and 0.015J/cm$^2$ and 0.007J/cm$^2$ (b) three different laser energy densities: 0.032J/cm$^2$ and 0.02J/cm$^2$ and 0.007J/cm$^2$.

According to Fig. 4(a), the UV-visible peaks for the number of the laser pulses at 1500 at three different laser energy densities: 0.032 J/cm$^2$ and 0.015 J/cm$^2$, and 0.007 J/cm$^2$ appeared at about λ= 405 nm and λ= 398 nm and λ= 406 nm, respectively.

According to description of Fig. 3(a), the size of Ag NPs at 0.015 J/cm$^2$ is the smallest of the three laser energy densities. In addition, the existence of one peak in the absorption spectrum refers to the existence of spherical shapes of particles in the laser radiation wavelength. Because absorption of energy is taken placed by surface electrons and the distribution of the electrons is uniform at the spherical surfaces. As a result, there is only one maximum absorption wavelength, and Ag NPs have not been formed at 0.007 J/cm$^2$. The optimum laser energy density for producing Ag NPs at the number of the laser pulses at 1500 was 0.015 J/cm$^2$.

According to the above (description of Fig.4(a)), the UV-visible peaks in Fig. 4(b) for the number of the laser pulses at 1500 at three different laser energy densities: 0.032 J/cm$^2$ and 0.02 J/cm$^2$, and 0.007 J/cm$^2$ appeared at about λ= 405 nm and λ= 399 nm and λ= 406 nm, respectively. As a result, the optimum laser energy density for producing Ag NPs at the number of the laser pulses at 1500 was 0.02 J/cm$^2$.

As shown in Figs. 3(a) and 3(b), the UV-visible peaks for the 900 numbers of the laser pulses at two optimum laser energy densities: 0.09 J/cm$^2$ and 0.11 J/cm$^2$, appeared at about λ= 404 nm and λ= 401nm, respectively. These peaks emerged from a localized surface Plasmon resonance of Ag NPs. Hence, they confirm that the Ag NPs have been formed in water. At ablation wavelength (λ=532 nm), self-absorption of radiation by solvent or metal NPs in the path of the radiant laser beam was low at higher laser energy densities. In addition, the laser beam penetration depth was high, and large NPs were separated from the surface of the target at higher laser energy density [19-21].

Consequently, the peak intensity of the UV-visible spectrum increased when the laser energy density increased. The increase in the absorption peaks can be related to the increase in concentration of Ag NPs at higher laser energy density.

As shown in Figs. 4(a) and 4(b), the UV-visible peaks for the optimum number of the laser pulses at 1500 at two optimum laser energy densities: 0.015 J/cm$^2$ and 0.02 J/cm$^2$, appeared at about λ=398 nm and λ=399 nm, respectively. The peak intensity of the UV-visible spectrum increased when the laser energy density increased. As the number of laser pulses light went up, the peak intensity of the UV-visible spectrum did so. As a result, the average size of the Ag NPs decreased along with a decline in the number of laser pulses light.

Figures 5 and 6 demonstrate TEM images of Ag NPs at two optimum laser energy densities for two optimum numbers of the laser pulses at 900 and 1500, respectively.

[ Downloaded from ijop.ir on 2026-11-24 ]

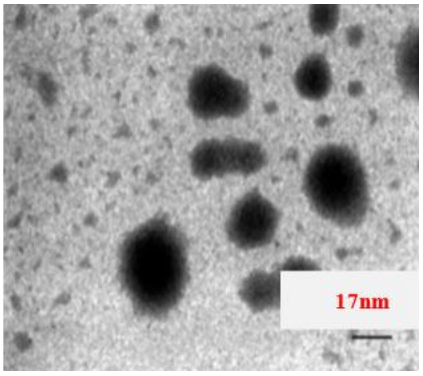


(a)

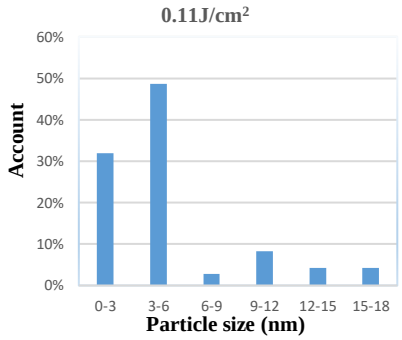


(b)

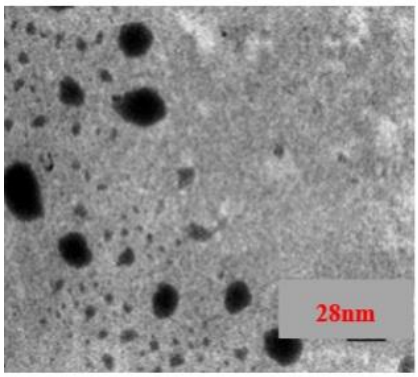


(c)

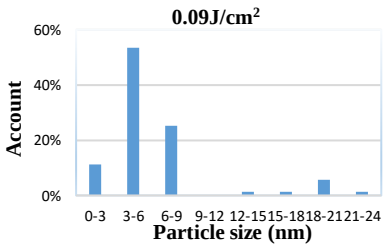


(d)

Fig. 5. TEM results of Ag NPs at the optimum number of the laser pulses at 900 at two optimum laser energy densities: (a) 0.11J/cm$^2$ (Scale Bar=17nm), (b) distribution diagram of Ag NPs for the optimum laser energy density at 0.11J/cm$^2$ (N=72, mean=5.04nm), (c) 0.09J/cm$^2$ (Scale Bar=28nm) and (d) distribution diagram of Ag NPs for the optimum laser energy density at 0.09J/cm$^2$ (N=71, mean=6.34nm).

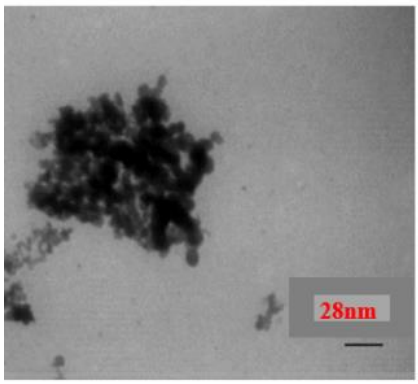


(a)

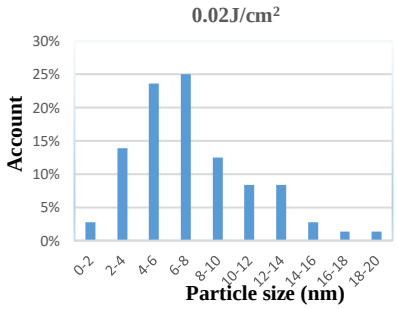


(b)

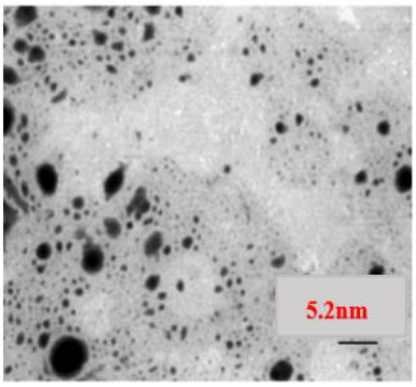


(c)

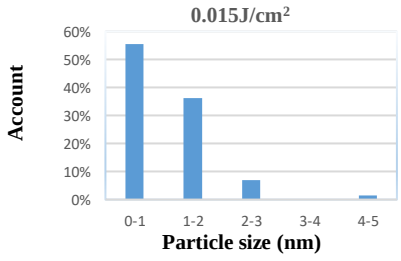


(d)

Fig. 6. TEM results of silver NPs at the optimum number of the laser pulses at 1500 at two optimum laser energy densities: (a) 0.02J/cm$^2$ (Scale Bar=28nm), (b) distribution diagram of Ag NPs for the optimum laser energy density at 0.02J/cm$^2$ (N=72, mean=7.34nm), (c) 0.015J/cm$^2$ (Scale Bar=5.2nm) and (d) distribution diagram of Ag NPs for the optimum laser energy density at 0.015J/cm$^2$ (N=72, mean=1.15nm).

According to Figs. 5 and 6, the average size of the Ag nanoparticles at the number of the laser

[ Downloaded from ijop.ir on 2026-11-24 ]

pulses at 900 in the laser energy density, F=0.11 J/cm$^2$, for 72 number of the Ag nanoparticles is 5.04nm, and for the laser energy density, F=0.09 J/cm$^2$, for 71 number of the Ag nanoparticles is 6.34nm. In addition, the average size of the Ag nanoparticles at the number of the laser pulses at 1500 at the laser energy density, F=0.02 J/cm$^2$, for 72 number of the Ag NPs is 7.34nm, and for the laser energy density, F=0.015 J/cm$^2$, for 72 number of the Ag NPs is 1.15nm. As can be seen from Figs. 5 and 6, the Ag NPs are almost spherical shapes in all samples and the size and size distribution have depended on the number of the laser pulses and the laser energy density [20, 21].

By comparing the Figs. 5 and 6, we found that the average size of the Ag NPs at the number of the laser pulses at 1500 is smaller than that of the Ag NPs at the number of the laser pulses at 900. Furthermore, the distribution of the Ag NPs at the number of the laser pulses at 1500 is more than that of the Ag NPs at the number of the laser pulses at 900. This is in agreement with the observation of the UV-visible spectrum at Figs. 3(a), 3(b), 4(a) and 4(b).

### B. *Nonlinear refractive index measurements (closed aperture Z-scan method)*

The Z-scan method used to measure the nonlinear parameters of Ag NPs in distilled water. The laser used is a continuous-wave diode-pumped laser Nd: YAG with $\lambda$=532nm. The sample was moved by a stepper motor along the z-axis with a step size of 0.1mm. The laser intensity at the focus of the converging lens at Z-scan method, $I_0$, is 8-15 W/cm$^2$

Figures 7(a) and 7(b) show the normalized transmittance, $\Delta T(z)$, for Ag NPs produced with the 900 numbers of the laser pulses for laser energy densities of 0.09 J/cm$^2$ and 0.11 J/cm$^2$, respectively.

Figures 8(a) and 8(b) show the normalized transmittance, $\Delta T(z)$, for Ag NPs produced with the 1500 numbers of the laser pulses for laser energy densities of 0.015J/cm$^2$ and 0.02J/cm$^2$, respectively.

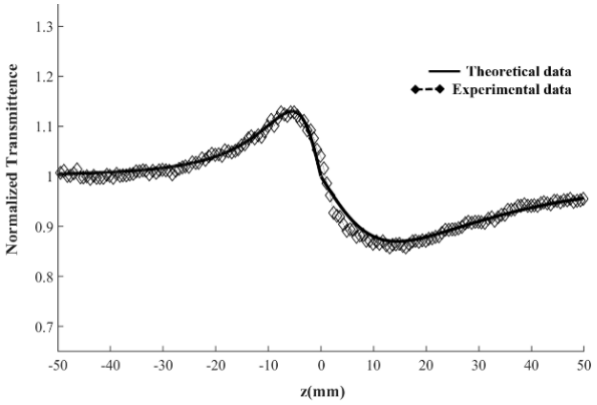


(a)

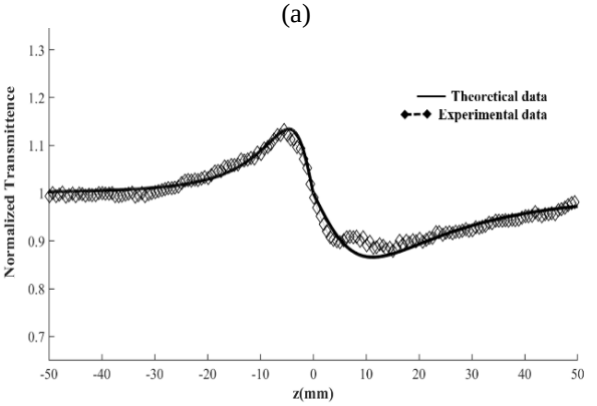


(b)

Fig. 7. Closed aperture Z-scan experimental data (dashed-diamond line) and theoretical curve (solid line) calculated using Eq. 2 for Ag NPs at the optimum number of the laser pulses at 900 with two optimum laser energy densities: (a) 0.09J/cm$^2$ and (b) 0.11J/cm$^2$.

The nonlinear phase shift, $\Delta\varphi_0$, gained after fitting Eq. 2 (solid line) to the experimental data (dashed-diamond line). The nonlinear refractive index of the Ag NPs in distilled water gained from Eq. 3 for optimum energy density [22]. The existence of one peak before the focal point, and one valley after the focal point in Figs. 7 and 8 demonstrate a negative nonlinear refractive index or self-defocusing effect. According to Figs. 3(a), 3(b), 4(a) and 4(b), the Ag NPs consisted of the substantial absorption around the $\lambda = 532nm$ (532nm is the excitation laser wavelength in the Z-scan method). Consequently, the observed nonlinearity effect in Figs. 7 and 8 may be due to the thermal effect. Since the amount of sodium citrate is little in the water, we disregarded its effects on linear and nonlinear refractive and absorption coefficients.

[ Downloaded from ijop.ir on 2026-11-24 ]

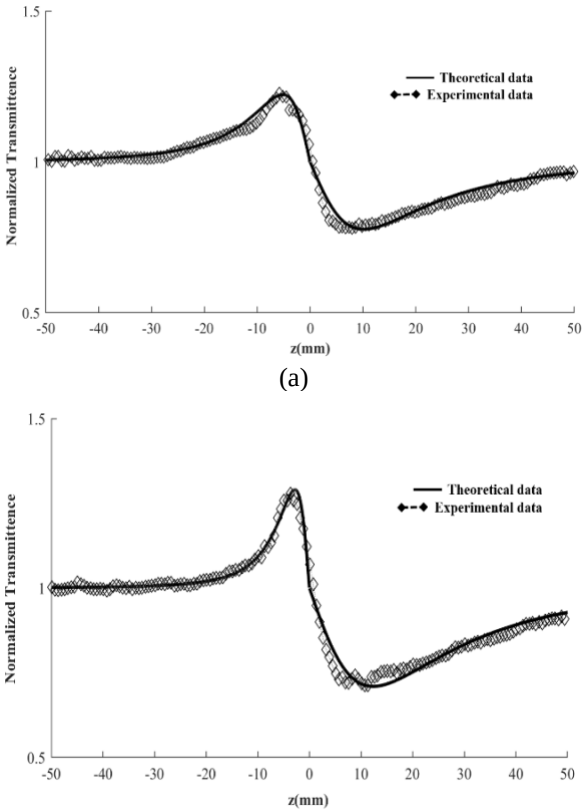


Fig. 8. Closed aperture Z-scan experimental data (dashed-diamond line) and theoretical curve (solid line) calculated using Eq. 2 for Ag NPs at the optimum number of the laser pulses at 1500 with two optimum laser energy densities: (a) 0.015J/cm$^2$ and (b) 0.02J/cm$^2$.

Table 1 displays the amounts of $\alpha_0$, $n_2$, $\beta$, $|W|$ $and$ $|T|$ and average size of Ag NPs for two numbers of the laser pulses at 900 and 1500 for four different laser energy densities. According to Table 1, the nonlinear refractive index increases as the number of laser pulses increases. The determined amounts of the two figures of merit $|w|$ and $|T|$ for the Ag NPs for the number of the laser pulses at 900 at two laser energy densities, 0.11 J/cm$^2$, and 0.09 J/cm$^2$, revealed that they are applicable tools for all-optical switching device.

.

Table **1.** The Amounts of $\alpha_0, n_2, \beta, |W|, |T|$ and average size of Ag NPs for two numbers of the laser pulses at 900 and 1500 nm for four different laser energy densities.

| Number of Laser pulses | Laser Energy Density (J/cm$^2$) | $\alpha_0$ (1/cm) | $n_2$ (cm$^2$/GW) | $\beta \times 104$ (cm/GW) | Average size of Ag NPs (nm) | $\|W\|$ | $\|T\|$ |
|---|---|---|---|---|---|---|---|
| 900 | 0.090 | 0.37 | - 3.48 | 3.59 | 6.34 | 1.5 | 0.52 |
| 900 | 0.110 | 0.28 | - 3.53 | 3.60 | 5.04 | 1.9 | 0.53 |
| 1500 | 0.015 | 1.07 | - 6.4 | -4.82 | 1.15 | 0.08 | 0.4 |
| 1500 | 0.020 | 0.26 | - 7.7 | 2.86 | 7.34 | 4.5 | 0.2 |

### C. *Nonlinear absorption coefficient measurements (opened aperture Z-scan method)*

Figures 9(a) and 9(b) show the normalized transmittance, $T(z)$, for Ag NPs produced for the 900 numbers of the laser pulses for laser energy densities of 0.09 J/cm$^2$ and 0.11 J/cm$^2$, respectively.

Figures 10(a) and 10(b) show the normalized transmittance, $T(z)$, for Ag NPs produced for the 1500 numbers of the laser pulses for laser energy densities of 0.015 J/cm$^2$ and 0.02 J/cm$^2$, respectively.

The nonlinear phase shift, $q_0(z)$, gained after fitting Eq. 4 (solid line) to the experimental data (dashed-diamond line). The nonlinear absorption coefficient of the Ag NPs in distilled water gained from Eq. 5 for optimum laser energy densities [22].

According to Figs. 3(a), 3(b), 4(a) and 4(b) (UV-visible spectrums), Ag NPs showed substantial absorption around $\lambda = 532nm$. These nonlinear absorptions presumably arise from two-photon absorption. The existence of a valley in the nonlinear absorption in Figs. 9(a), 9(b), and 10(b) indicate the existence of the two-photon absorption.

On the other hand, the data in Table1 show that nonlinear absorption coefficients have decreased with increasing NP size for NPs larger than 1.15 nm, which depends on the number of NPs in the measured volume at Z-scan method. As a result, the nonlinear

[ Downloaded from ijop.ir on 2026-11-24 ]

absorption coefficient has dependent on the concentration of Ag NPs and the laser energy density.

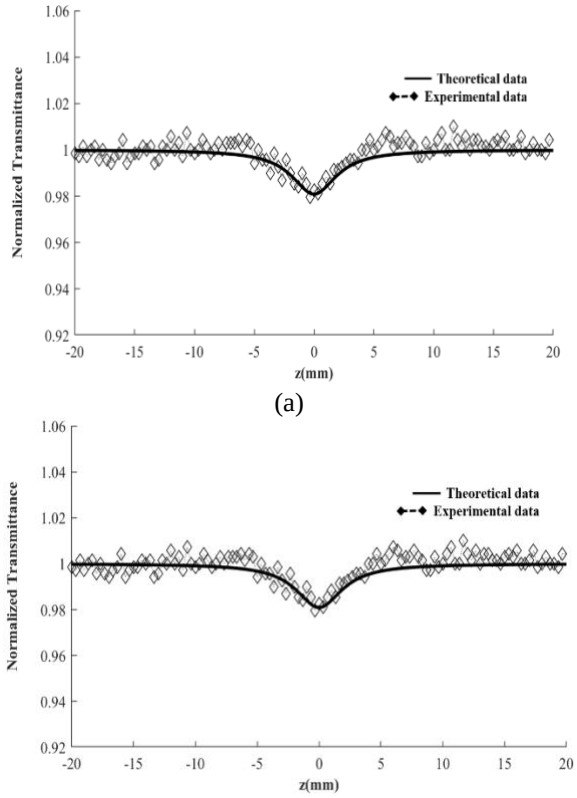


Fig. 9. Opened aperture Z-scan experimental data (dashed-diamond line) and theoretical curve (solid line) calculated using Eq. 4 for Ag NPs at the optimum number of the laser pulses at 900 with two optimum laser energy densities: (a) 0.09J/cm$^2$ and (b) 0.11J/cm$^2$.

On the other hand, the existence of one peak in nonlinear absorption in Fig. 10(a) shows the saturation of absorption. The saturable absorption behavior for these Ag NPs can be explained by surface-Plasmon resonance at 400nm, which led to an increasing in light transmittance through Ag NPs in water. Ag NPs exhibit an intense absorption peak at around 400nm due to an intraband sp→sp transition in Ag, which is strongly dependent on the size of Ag NPs. The electronic excitation has occurred because of intraband sp→sp transition at 532nm (the excitation wavelength at the Z-scan method). In addition, High energy photon absorption is considered to excite the Ag NPs at 532nm, which can lead to the equalization of electron papulation in occupied and unoccupied energy levels. As a result, the saturation absorption can be seen at 532nm, which has been displayed in Fig. 10(a) [23-26].

Since the Z-scan is a sensitive single-beam method, the smallest external factor causes chances in the data of the Z-scan device. Therefore, the fluctuations in Figs. 9 and 10, outside the main peak, are caused by the errors in the Z-scan setup.

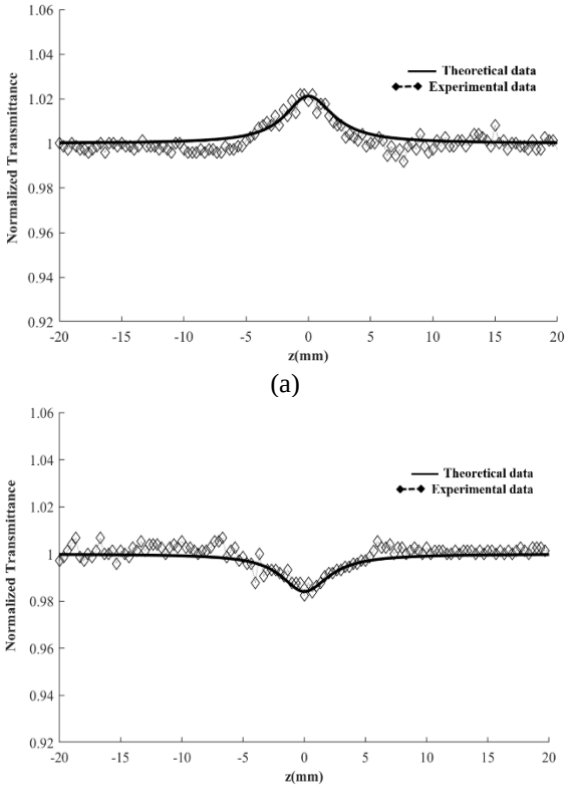


Fig. 10. Opened aperture Z-scan experimental data (dashed-diamond line) and theoretical curve (solid line) calculated using Eq. 4 for Ag NPs at the optimum number of the laser pulses at 1500 with two optimum laser energy densities: (a) 0.015J/cm$^2$ and (b) 0.02J/cm$^2$.

The determined amounts of two figures of merit ($|w| \gg 1$ and $|T| \ll 1$) for the Ag NPs in Table 1, for the 1500 numbers of the laser pulses and 0.02J/cm$^2$ laser energy density revealed that they are applicable tools for all-optical switching devices. Nonetheless, the determined amounts of the two merit figures ($|w| \ll 1$ and $|T| \ll 1$) for the Ag NPs in Table **1**, for the 1500 numbers of the laser pulses and 0.015J/cm$^2$ laser energy density revealed that they are not applicable tools for all-optical switching devices. Therefore, Ag NPs larger

[ Downloaded from ijop.ir on 2026-11-24 ]

than 1.15nm are applicable for all-optical switching devices.

## IV. CONCLUSION

In this study, Ag NPs have been produced using Nd: YAG laser ablation at λ=532nm at two optimum numbers of laser pulses (900 and 1500) at four optimum laser energy densities. The sodium citrate used to control the size of NPs capped $Ag^0$ and $Ag^+$ ions. According to UV-Visible spectrum and TEM images, the large Ag NPs were surface Plasmon peaks at large wavelengths. The intensity of the UV-Visible spectrum, as well as the distribution of the Ag NPs, increased when the number of laser pulses light increased. The size of Ag NPs can be controlled by increasing or decreasing the laser energy density according to the number of fixed laser pulses. The nonlinear refractive index and nonlinear absorption coefficient of the Ag NPs were investigated by the Z-scan method. The results of the nonlinear refractive index showed a negative value for each sample. This means that the samples act as a concave lens, and the thermal self-defocusing effect can be the main factor of nonlinear behavior. Nonlinear refractive index ($n_2$) increased when the number of laser pulses light increased. In addition, the nonlinear absorption coefficient (β) decreased when the number of laser pulses light increased. The average size of NPs is showed small values. As a result, the nonlinear refractive indices and nonlinear absorption coefficients show larger values than those previously reported in articles.

Moreover, the nonlinear absorption coefficient exhibited a two-photon absorption behavior, which explained by β dependence on the concentration of Ag NPs for Ag NPs larger than 1.15nm. The nonlinear absorption coefficient exhibited a saturable absorption behavior for Ag NPs equals to 1.15nm, which can explain by surface-Plasmon resonance at 400nm because of intraband sp→sp transition in Ag, which strongly has been dependent on the size of Ag NPs. As a result, the nonlinear absorption coefficient and nonlinear refractive index depend on the number of laser pulses and the laser energy density. According to the two figures of merit, the Ag NPs at the optimum number of the laser pulses, 900, are applicable tools for all-optical switching devices. This is due to the presence of delocalized π-electrons and the transforming of electron densities among the Ag NPs and other substances. However, for produced Ag NPs with the optimum number of the laser pulses, 1500, and the optimum laser energy density of $0.015 J/cm^2$, $|W|$ is less than one, indicating that these Ag NPs are not applicable tools for optical switching devices. Therefore, Ag NPs larger than 1.15nm are applicable tools for all-optical switching devices.

## ACKNOWLEDGMENT

We are deeply grateful to Urmia University for providing a fellowship for the present work.

## REFERENCES

**[1]** P.P. Atil, D.M. Phase, S.A. Kulkarni, S.V. Ghaisas, and S. Bogale, "Pulsed-laser–induced reactive quenching at liquid-solid interface: Aqueous oxidation of iron," Phys. Rev. Lett., Vol. 58, pp. 238-241,1987.

**[2]** L. Francois, M. Mostsfavi, J. Belloni, and P. Feneyrou, "Optical Limitation induced by Gold Clusters. 1. Size Effect," J. Phys. Chem. B., Vol. 3, pp. 4965-4971, 2001.

**[3]** R.B. Martin, M.J. Meziani, and S. Perera, "Optical limiting of silver-containing nanoparticles," Opt. Mater., Vol. 29, pp. 788-793, 2007.

**[4]** R.A. Ganeev, S.R. Kodirov, and A.I. Kamalov, "Nonlinear optical parameters of colloidal silver at various stages of aggregation," Tech. Phys., Vol. 72, pp. 889-893, 2002.

**[5]** J.R. Gonzalez-Castollo, and E. Rodriguez-Gonzalez, "Assisted laser ablation: silver/gold nanostructures coated with silica," Appl. Nanosci., Vol. 7, pp. 597-605, 2017.

**[6]** F. Hajiesmaeilbaigi, A. Mohammadalipour, S. Hoseinkhani, and H.R. Fallah, "Preparation of silver nanoparticles by laser ablation and fragmentation in pure water," Laser Phys. Lett., Vol. 3, pp. 252-256, 2006.

**[7]** B. Calderen-Jimenez, and A.R. Montoro Bustos, "Silver Nanoparticles: Technical Advances, Societal Impact, and Metrological

[ Downloaded from ijop.ir on 2026-11-24 ]

Challenges", J. Nature, Scientific reports, Vol. 12, pp. 1-18, 2022.

**[8]** A. Nicolae-Maranciuc and D. Chicea, "Ag Nanoparticles for Biomedical Applications— Synthesis and Characterization— A Review," Int. J. Mol. Sci. Vol. 23, pp. 1-30, 2022.

**[9]** Q. Chen, Y. Ye, and J. Liu, "Stability Evolution of Ultrafine Ag Nanoparticles Prepared by Laser Ablation in Liquids," J. Colloid Interface Sci., Vol. 585, pp. 444–451, 2021.

**[10]** R.E. De Góes, M. Muller, and J. Fabris, "Spectroscopic detection of glyphosate in water assisted by laser-ablated silver nanoparticles," J. Sensors, Vol. 17, pp. 1-15, 2017.

**[11]** A.R. Sadrolhosseini, A.S.M. Noor, and N. Farraji, "Optical Nonlinear Refractive Index of Laser-Ablated Gold Nanoparticles Graphene Oxide Composite," Hindawi, J. Nanomaterials, Vol. 2014, pp. 1-8, 2014.

**[12]** A. Jafari, B. Zeynizadeh, and S. Darvishi, **"**Study of linear and nonlinear optical properties of nickel immobilized on acid-activated montmorillonite and copper ferrite nanocomposites," J. Molecular Liquid, Vol. 253, pp. 119-126, 2018.

**[13]** A. Pyatenko, K. Shimokawa, and M. Yamaguchi, "Synthesis of silver nanoparticles by laser ablation in pure water," Appl. Phys. A, Vol. 79, pp. 803-806, 2004.

**[14]** A.R. Sadrolhosseini, M.A. Mahdi, F. Alizadeh, and S. Abdul Rashid, "Laser Ablation Technique for Synthesis of Metal Nanoparticle in Liquid," IntechOpen, Laser Technol. its Appl., DOI: 10.5772/intechopen.80374, 2018.

**[15]** A.G. Rad, H. Abbasi, and K. Golyari, "Fabrication and Nonlinear Refractive Index Measurement of Colloidal Silver Nanoparticles," Appl. Phys. Math., Vol. 2, pp. 135-139, 2012.

**[16]** M.S. Bahae and D.J. Hagan, "Sensitive measurement of optical nonlinearities using a single beam," IEEE, J. Quantum electron., Vol. 26, pp. 760-769, 1990.

**[17]** H.L. Fan, Q. Ren, X.Q. Wang, and J. Sun, "Investigation on Third-Order Optical Nonlinearities of Two Organometallic Dmit2-Complexes Using Z-Scan Technique," J. Natural Science, Vol. 1, pp. 136-141, 2009.

**[18]** P. Sivakumar, R. Ramesh, A. Ramanand, and S. Ponnusamy "Synthesis and characterization of NiFe 2O 4 nanosheet via polymer assisted co-precipitation method," J. Mater. Lett., Vol. 65, pp. 483-485, 2011.

**[19]** M.M. Koebel, C.L. Jones, G.A. Bowmaker, "Distinguishing molecular environments in supported Pt catalysts and their influences on activity and selectivity," J. Nanopart. Res., Vol. 10, pp**.** 1063–1069, 2008.

**[20]** M. Mashayekh and D. Dorranian, "Third Order Optical Nonlinearity of Silver Nanoparticles Prepared by Chemical Reduction Method." Optik -Int. Light Electron Opt., Vol. 125, pp. 5612-5618, 2017.

**[21]** M.I.S. Tan and A.F. Omar, "State of the Art in Gold Nanoparticle Synthesisation via Pulsed Laser Ablation in Liquid and Its Characterization for Molecular Imaging: A Review," J. Results Phys., Vol. 14, pp. 1-20, 2019.

**[22]** H. Aleali and N. Mansour, "Nonlinear Responses and Optical', Limiting Behavior of Ag Nanoparticle Suspension," J. Science, I. R. Iran, Vol. 21, pp. 273-278, 2010.

**[23]** Y. Z, j. X, W. Z, "Measurements of Particle Size Distribution Based on Mie Scattering Theory and Markov Chain Inversion Algorithm"**,** Semantic scholar, J. Software, Vol. 7, pp. 2309-2316, 2012.

**[24]** S. K. Maurya, A. Rout, R. A. Ganeev, "Effect of Size on the Saturable Absorption and Reverse Saturable Absorption in Silver Nanoparticle and Ultrafast Dynamics at 400 nm", Hindawi, J. Nanomaterials, Vol. 2019, pp. 1-12, 2019.

**[25]** R. Philip, P. Chantharasupawong, H. Qian, R. Jin, and J. Thomas, "Evolution of nonlinear optical properties: from gold atomic clusters to plasmonic nanocrystals," J. Nano Letters, Vol. 12, pp. 4661–4667, 2012.

**[26]** C. M. Aikens, S. Li, and G. C. Schatz, "From discrete electronic states to plasmons: TDDFT optical absorption properties of Agn (n=10, 20, 35, 56, 84, 120) tetrahedral clusters," J. Physical Chemistry C, Vol. 112, pp. 11272–11279, 2008.

[ Downloaded from ijop.ir on 2026-11-24 ]



**Bita Azmoodeh Afshar** was born in Urmia in 1979. She was graguated from Tabriz University in M.Sc. at Atomic and Molecular Physics Major in 2011. She is now studying PhD in Optics and Laser at Urmia University.

Her research fields are about Synthesis of Nanoparticles by laser ablation and investigation of nonlinear optical properties of nanoparticles by Z-scan method. Also, she was designed Dye-sensitized solar cells by inserting single-walled carbon nanotubes for obtaining high Efficiency.



**Akbar Jafari** is a profsser of optics and laser in Physics Department, Urmia University**.** He was graguated from Tabriz University in Ph.D. at Atomic and Molecular Physics Major in 2008. His research fields are about investigation of nonlinear optical properties of substances. Also, he was designed and launched the Z-scan method.



**Mir Maqsood Golzan** is a profsser of Plasma, Physics Department, Urmia University**.** He had been graguated from Tehran University in M.Sc. at Physics Major In 1980. Also, He was graguated from Sydney University in Ph.D. at Applied Physics Major in 1995.

His research fields are about investigating electrochemical properties of composite thin films and ultrasonic behaviors on geramination



**Rahim Naderali** is assistant professor of Urmia University**.** He is the head of the Science Faculty. He had been graguated from Tabriz University at Atomic and Molecular Physics in M.Sc. major in 1999. Also, he was graguated from Urmia University at Atomic and Molecular Physics in Ph.D. Major in 2009.

His research fields are about investigation of nonlinear optical properties of quantum dots and design of Plasma Antenna with changing the frequency.

[ Downloaded from ijop.ir on 2026-11-24 ]

**THIS PAGE IS INTENTIONALLY LEFT BLANK.**

[ Downloaded from ijop.ir on 2026-11-24 ]